Fatigue Behaviour of Aluminium Members with Different Notch Root Shapes

Buljan, Nebojša; Skejić, Davor; Krolo, Paulina; Lukić, Mladen

Article

Fatigue Behaviour of Aluminium Members with Different Notch Root Shapes

Nebojša Buljan [1,*], Davor Skejić [2], Paulina Krolo [3] and Mladen Lukić [4]

1   RI ISA d.o.o., Kapitanovo 25, 51000 Rijeka, Croatia
2   Department for Structures, Faculty of Civil Engineering, University of Zagreb, Fra Andrije Kačića-Miošića 26, 10000 Zagreb, Croatia; davor.skejic@grad.unizg.hr
3   Department of Structural Engineering and Technical Mechanics, Faculty of Civil Engineering, University of Rijeka, Radmile Matejčić 3, 51000 Rijeka, Croatia; paulina.krolo@gradri.uniri.hr
4   Centre Technique Industriel de la Construction Métallique (CTICM), Espace Technologique, Route de l'Orme des Merisiers, 91193 Saint-Aubin, France; mlukic@cticm.com
*   Correspondence: n.buljan@permasteelisagroup.com

Abstract: In unitised curtain walls, the transfer of horizontal loads, mainly wind loads, from the upper into the lower unit is achieved through the head/notch interlocking connection. Optimisation of the machining process would require a sharp root of the notch, causing an increase in the stress concentration. In order to predict fatigue resistance during design life, the influence of the radius at the root of the notch has been tested in both static and cyclic regimes. The cyclic regime is based on the load history equivalent of 50 years of wind exposure. Numerical simulations on the test assembly have been conducted in order to verify their adequacy for future research on similar issues. The experimental results demonstrated that, for the given specimen shape and alloy, a sharp notch would not lead to premature failure, and such a detail is safe from the purview of damage-tolerant design.

Keywords: notch; aluminium profile; fatigue; wind action; stress concentration; unitised curtain wall

1. Introduction

Aluminium structural alloys are applied in a wide field within the construction industry [1]. One of their major applications in buildings is related to façades constructed as unitised curtain walls, which substitute for traditional external walls. A curtain wall consists of prefabricated units, typically one floor high, composed of loadbearing aluminium frames and infill, and completed with an external and internal finish (Figure 1). Units are interlocked horizontally with male/female mullion halves.

The deadload of each unit is supported by brackets fixed to the main structural frame of the building at the floor level: one row of brackets per one row of units. In order to avoid the transfer of vertical loads from the main structure into the curtain wall, each horizontal row of units is connected to other rows by stack joints, allowing vertical movements independently of other rows by using available movement gaps between rows. The transfer of horizontal loads, mainly caused by wind pressure and suction, from the upper row to the lower row relies on interlocking between units at stack joints, thus creating a Gerber beam over the height of the building.

One of the common interlocking principles is the engagement of a "chicken head" feature in the transom of the lower unit into the notch in the mullion of the upper unit. The notch is exposed to the horizontal load at its tip, where the load (Figure 2) is transferred through the contact point from the vertical mullion of the upper unit to the chicken head of the lower unit. The notch is a stress riser, and the highest stress concentration occurs at the root of the notch.
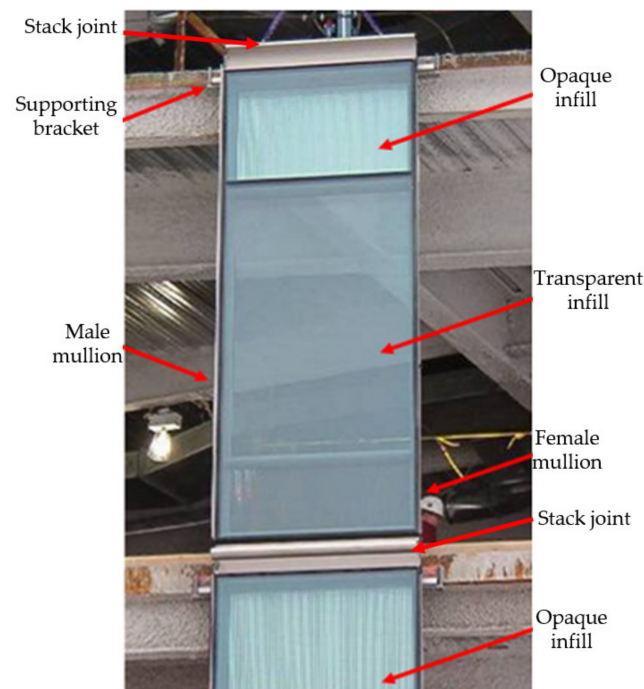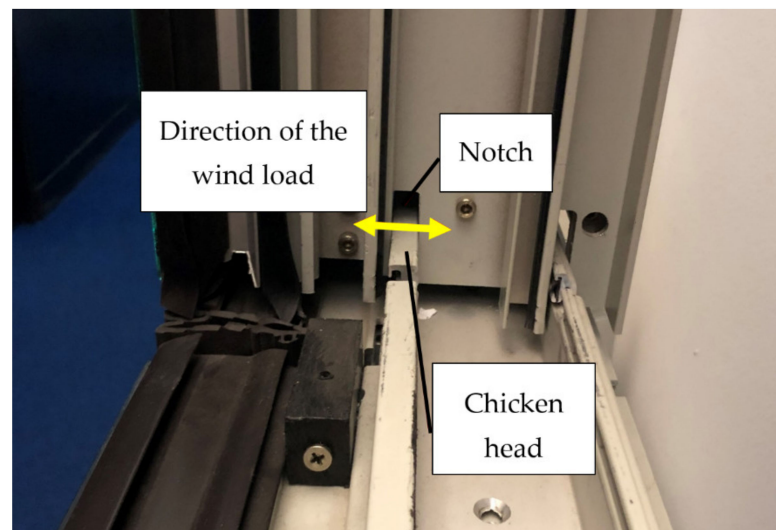
Figure 1. Typical curtain wall unit.

Figure 2. Stack joint between vertical units of a curtain wall.

The production of curtain walls is an industrial process which is constantly being optimised. A possible optimisation investigated here is an alternative machining of the notch in the aluminium profile by sawing in lieu of the traditionally used milling machining process. Sawing may result in a reduction in the machining time, resulting in more economical production, in particular, for large projects where tens of thousands of profiles are machined. However, the problem is that sawing results in sharp corners at the notch, which are exposed to repeated wind loads throughout the design life.

The notch with sharp corners is generally known to be susceptible to fatigue failure when exposed to the cycling load. This detail is strongly advised against in the literature [2–4] due to the high stress concentration, which is supposed to be mitigated by rounding the sharp corner.

The phenomenon of fatigue in aluminium structures is not widely researched. Moreover, aluminium structures susceptible to fatigue exhibit some particularities when com-

pared to steel structures [5]. The scope of this research is to investigate the fatigue behaviour of a sharp notch as obtained by sawing into an aluminium structural element in the façade of the building exposed to wind action during its 50-year design life.

A crack may nucleate from a sharp notch rather quickly due to elevated stress at the notch root. Since the deformation at the notch root is plastic, the crack initiates under conditions of local plasticity. For cracks growing into the plastic stress–strain field of a notch, the rate of the crack growth is initially high, but decreases as the crack grows further away from the notch root. As the crack exceeds 10–20% of the notch radius, the notch geometry has little influence on the stress–strain field of the advancing crack and can stop growing once it has grown out of the notch-influenced region [6]. If the crack keeps growing, it may grow into the elastic zone (Figure 3). Crack growth through a notch stress–strain field may represent a major or minor portion of the total fatigue life [7]. After the crack grows out of the plastic zone, it may grow to become significantly long.
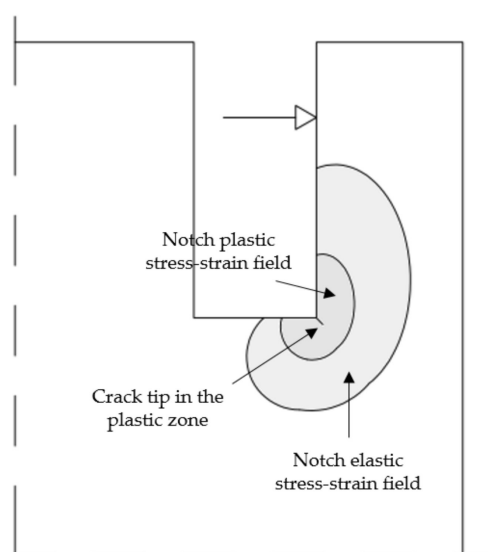

Figure 3. Phenomenology of crack growth through a notch stress–strain field.

The aim of this research is to investigate whether a sharp root notch is nevertheless a technically viable design for the entire design life of a façade, within given geometry and for known load history. The load history chosen for this research, representing a 50-year wind exposure, was described by N.J. Cook [8] (Appendix K, Table 1).

For comparison, three different characteristic geometries for the notch were obtained through different machining techniques, and these were both tested and numerically simulated. The notch dimensions remained constant, but the shape of the root of the notch varied: sharp corners, rounded corners, and the full semi-circular root.

2. Experimental Study

2.1. General

An experimental programme was conducted at the structures laboratory of the Faculty of Civil Engineering, University of Rijeka [9]. Specimens were tested using the horizontally positioned servo-hydraulic actuator Zwick/Roell with a capacity of 250 kN. A total of 12 tests on mullion samples were performed, of which 5 specimens were tested under monotonic loading and 7 specimens under cyclic loading.

It was known that the most structurally resilient root shape in this case would be a semi-circle with a diameter equal to the width of the notch (Figure 4c). Due to a requirement to minimise the cross-section of the frame, the semi-circular root was not practical, as it would reduce the available vertical gap for the movement, as discussed later. Hence, root corners were rounded with a radius equal to the radius of the milling bit, typically close to the thickness of the aluminium wall (Figure 4b), which corresponds to the diameter of the

smallest bit typically used for the milling of aluminium. Machining by sawing results in sharp corners on the notch (Figure 4a), which is known to be the worst condition for stress concentration. All three geometries of the notch (Figure 4) were tested, and the results were compared to numerical models. It is important to note that the width of the notches was constant, but the shape of the root of the notches was variable: sharp corners, rounded corners, and the full semi-circular root.
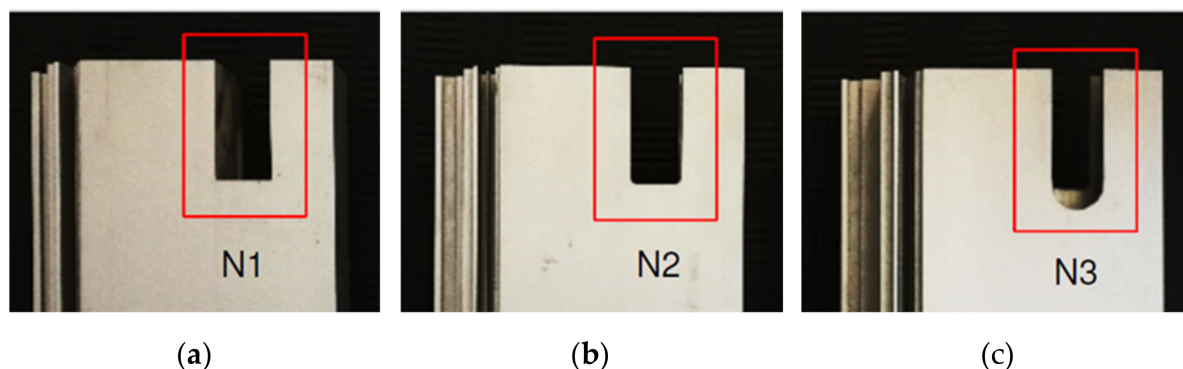

(a) (b) (c)

Figure 4. Shape of root notch: (**a**) sharp, N1, (**b**) rounded, N2, (**c**) semi-circular, N3.

2.2. Material and Specimen Geometry

The material used was the aluminium alloy EN AW 6063 T6 (extrusion) [10]. Producer certificates confirmed the chemical composition to be compliant with requirements for the alloy. The surface finish of specimens was natural anodised. Despite the fact that statistical data for mechanical properties of the used alloy can be found in the most recent literature [11], tension tests on used profiles were carried out for verification purposes. In order to validate the mechanical properties of the material, 3 dog-bone coupons were tested in accordance with the provisions of EN ISO 6892-1 [12]. Dog-bone coupons Al1 through Al3 were obtained by cutting out of the wall of the single profile. The measured mechanical properties were compared to values from EN 755-2 [10] as well as values provided by the materials supplier (Table 1).

Table 1. Comparison of mechanical properties.

Coupon/Source	$R_{p0,2}$	R_m	A
	[MPa]	[MPa]	[%]
Coupon Al1	207.7	229.8	10.1
Coupon Al2	211.0	233.7	8.0
Coupon Al3	222.1	241.9	9.7
EN 755-2 [6]	170.0	215.0	8.0
Supplier's certificate	216.6	235.7	11.8

The profile used was the male half of the split mullion (Figure 5a), an aluminium extrusion with an asymmetric cross-section. The inner wall of the section parallel to the notched wall was continuously cut for the entire length of the specimen, as shown in Figure 5b, so that the inner wall did not contribute to the loadbearing capacity of the notch.

The geometry of the notches is shown in Figure 6. The width of the notch was 25 mm, which enabled a close fit of the chicken head. The depth of the notch was 55 mm. This enabled ±20 mm of vertical movement in the stack joint.
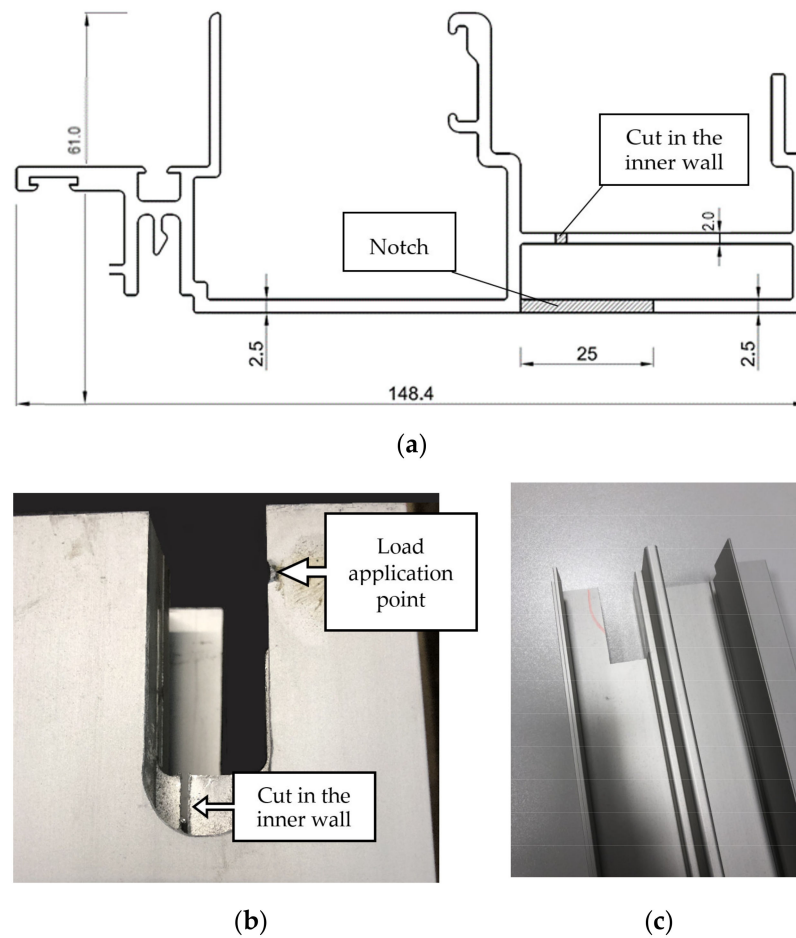
(a)

(b)   **(c)**

Figure 5. (**a**) Cross-section of the profile, (**b**) semi-circular notch in the profile, (**c**) view of the profile.

(a)   **(b)**   **(c)**
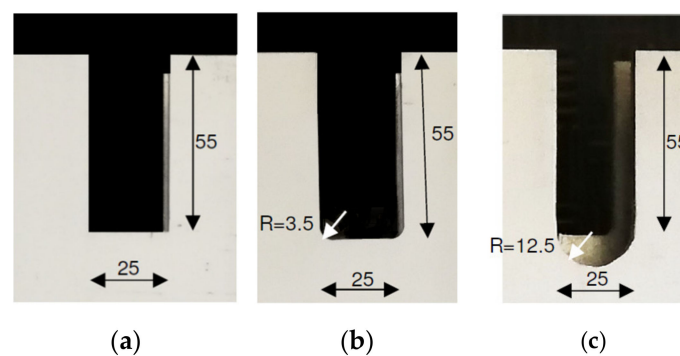
Figure 6. Geometry of the (**a**) sharp notch, N1, (**b**) rounded notch, N2, and (**c**) semi-circular notch (mm).

It should be noted that the total depth of the semi-circular notch was 67.5 mm, which allowed for a straight length of 55 mm plus a radius of 12.5 mm for the semi-circle. In practice, the semi-circular notch was not used due to geometric constraints. The vertical section through the stack joint between two façade units is shown in Figure 7a. The enlarged detail in Figure 7b shows the vertical movement capacity of the stack joint when the gap between two units closes. The grey chicken head shows the nominal position as-designed. The blue chicken head shows the closed position if the rounded notch was used. The red chicken head shows the closed position if the semi-circular notch was used. It can be observed that the movement capacity of the semi-circular notch (sc) was smaller than that of the rounded notch (rnd), as the movement of the chicken head was limited by the contact

with the semi-circular notch (red contour in Figure 7). The position of the semi-circular notch would need to be higher to enable the same movement capacity as the rounded notch, but this is not possible, as, in that case, the semi-circular part of the notch would protrude over the horizontal transom and enter the area visible to the user (green hole in Figure 7), leaving it open for the passage of air and water into the building. However, the semi-circular notch was investigated as well for comparison. For test, specimens with a semi-circular notch at a total depth of 67.5 mm were used. Numerical modelling was performed for both semi-circular geometries, at 55 mm and 67.5 mm of the notch depth.
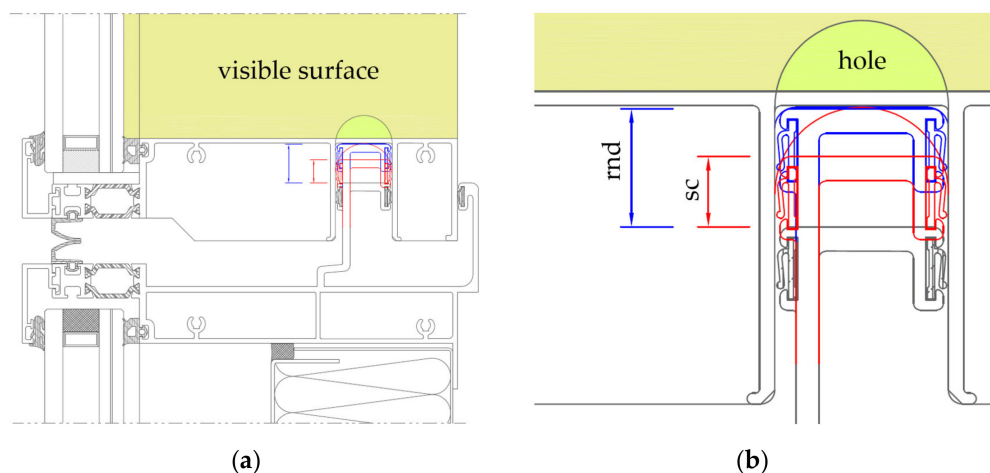

(a)   (b)

Figure 7. (**a**) Stack joint; (**b**) enlarged detail showing the vertical movement capacity.

2.3. Monotonic Testing

Prior to the cyclic tests, profile specimens were tested by applying a monotonically increasing point load until failure. Tests were carried out under displacement control. The scope of the monotonic testing was to assess the ultimate load to be used as the basis for the load history in cyclic testing. Specimen profiles were 730 mm long with a notch at one end. In total, five specimens were tested (see Table 2).

Table 2. Description of test specimens.

Specimen Monotonic Test	Cyclic Test	Shape of Notch N	Width of Notch (mm)	Depth of Notch (mm)	Radius at the Root of Notch (mm)
M_N1_1	C_N1_1				
M_N1_2	C_N1_2	Sharp (N1)		55	0
-	C_N1_3				
M_N2_1	C_N2_1		25		
M_N2_2	C_N2_2	Rounded (N2)		55	3.5
M_N3	C_N3_1	Semi-circular		67.5	12.5
-	C_N3_2	(N3)			

The specimen was held in the steel frame (Figure 8b) at two points 355 mm apart, and the horizontal load F was applied at the top end of the profile (Figure 8a).

The point of application for load F was 15 mm below the top end of the profile, forming a 360 mm structural cantilever. The tests were conducted by gradually increasing the applied load under displacement control of the actuator at a constant speed of 0.025 mm/s until the specimen fractured.

The deformation of the specimen was measured in 6 positions. The measurement data was collected using a datalogging device that recorded all measurements at 0.01 s intervals. Displacements were measured using Linear Variable Displacement Transducers (LVDT) with an accuracy of 0.2%, as shown in Figure 9.
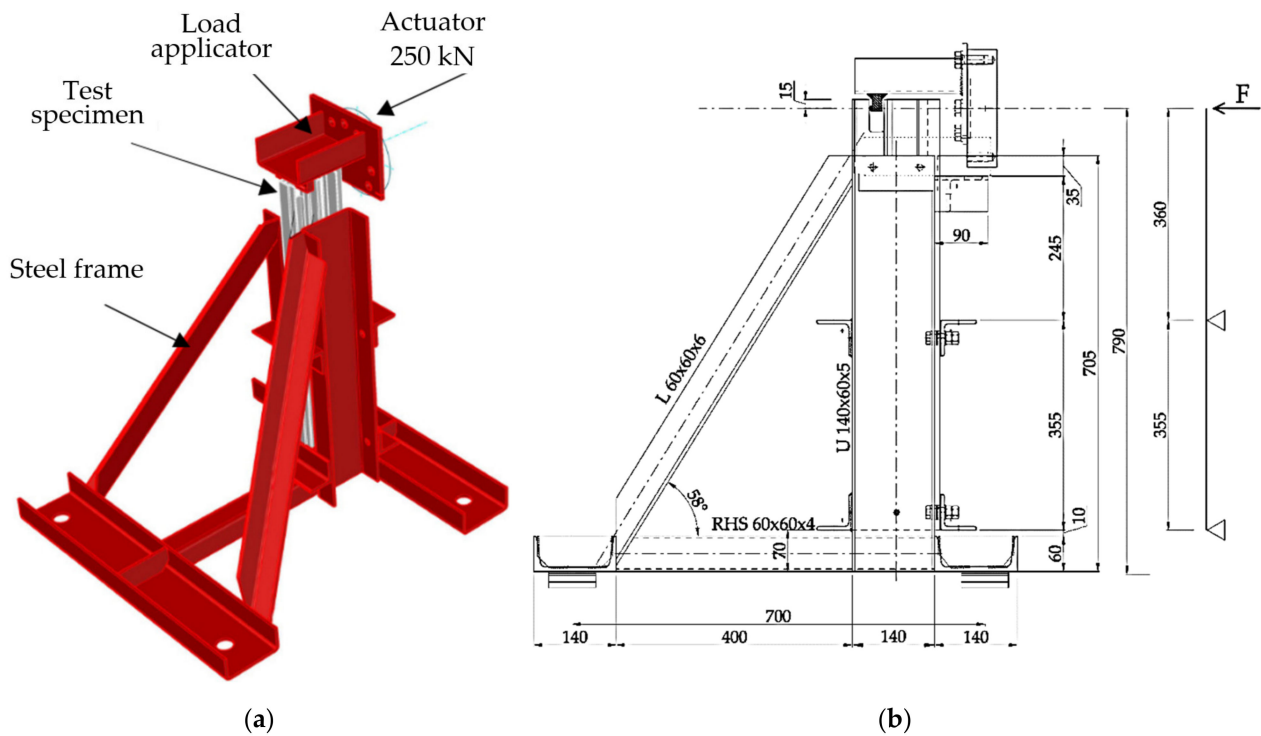
Figure 8. (**a**) Test setup; (**b**) test frame and the structural system (mm).
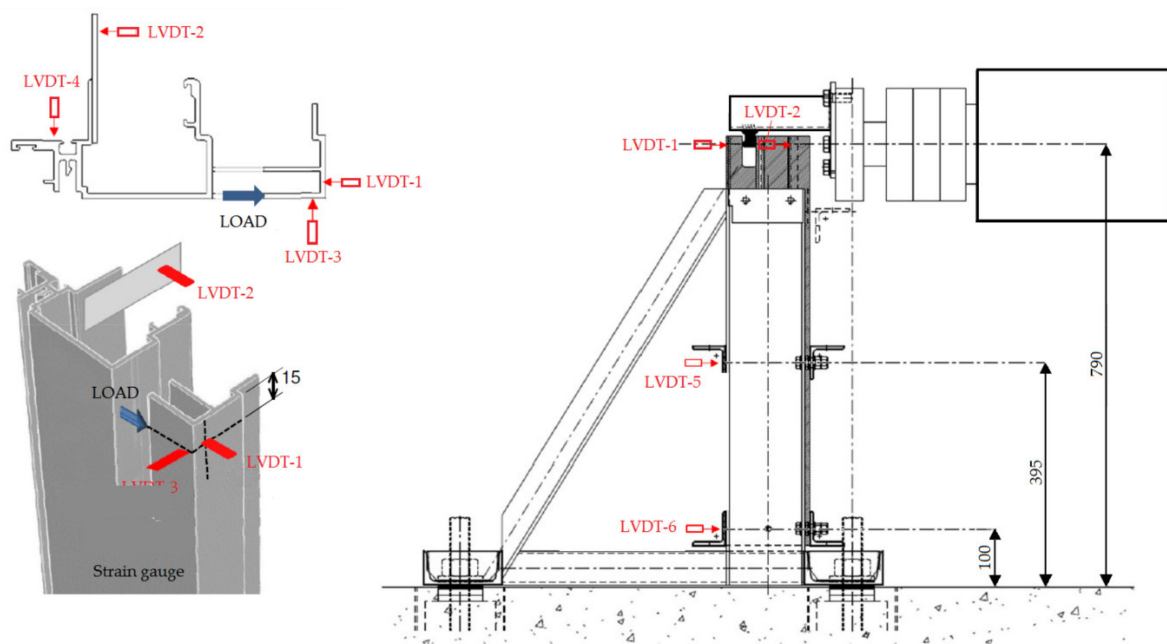

Figure 9. Positions of LVDTs.

The scope of LVDTs:

- LVDT-1,2,3,4 were located at the level of the application of the load.
- LVDT-1—absolute displacement at the back of the profile behind the notch in the direction of the load.
- LVDT-2—absolute displacement at the tip of the specimen in the direction of the load
- The differential of LVDT-1 − LVDT-2 measures the opening of the notch under the load.
- LVDT-3—absolute displacement at the back of the profile behind the notch perpendicular to the direction of the load.

- LVDT-4—absolute displacement at the top end of the specimen perpendicular to the direction of the load.
- The differential of LVDT-3 − LVDT-4 measures the rotation of the tip of the specimen under load.
- LVDT-5—absolute displacement of the upper support of the specimen in the direction of the load (upper angle in the steel frame).
- LVDT-6—absolute displacement of the lower support of the specimen in the direction of the load (lower angle in the steel frame).
- The displacements of LVDT-5 and LVDT-6 are used to confirm the sufficient stiffness of the supporting steel frame.
- The differential of LVDT-5 − LVDT-6 determines the rotation of the supporting steel frame in order to distinguish between movement at the tip of the specimen due to the rotation of the support and movement due to the bending of the specimen.

The main results of the testing are tabulated in Table 3.

Table 3. Results of the monotonic testing.

Specimen	Ultimate Load (kN)	Opening of the Notch LVDT-1 − LVDT-2, Figure 8. (mm)
M_N1_1	6.78	6.18
M_N1_2	6.99	3.78
M_N2_1	8.08	9.49
M_N2_2	8.61	9.45
M_N3	8.45	20.20

It should be noted that specimens with the sharp notch (Figure 10a), as expected, had lower breaking forces (6.78 kN and 6.99 kN), which was, on average, 82% of the breaking force for specimens with rounded or semi-circular notches (8.08 kN, 8.61 kN, and 8.45 kN). Since the opening of the notch was measured at the time of the fracture, there was a notable difference for various specimens. This value depended on the mode of the breakage and comprised localized plastic effects; for M_N3, this value was highest as the wall buckled, which can be seen in Figure 10b.

(**a**)　　　　　　　　　　　　　　　(**b**)

Figure 10. Fracture in monotonic tests: (**a**) Sharp notch specimen M_N1_1; (**b**) Semi-circular specimen M_N3.

Specimens with the sharp notch failed through the crack at the root of the notch due to the concentration of tensile stress (Figure 10a). Specimens with the rounded or semi-circular notch experienced local buckling of the aluminium wall at the load application point prior to the fracture, so the material at the root of the notch was exposed to the combined stress due to the rotation of the aluminium wall (Figure 10b). The rotation of the aluminium wall was a secondary effect caused by the buckling of the wall, which shifted the application point of the load out of the plane of the wall.

The lower maximal measured force for the specimen with the sharp notch was taken as the basis for the load history of subsequent cyclic testing.

2.4. Cyclic Testing

2.4.1. Load History

The dominant action on the curtain wall is wind action. During the design life of a building (usually 50 years), the notch is exposed to cycles of the horizontal load caused by wind action on the curtain wall. Although the tested specimens were taken from a real project, the scope of the test was not to verify the adequacy of the aluminium structural element for the design load for that specific project, but rather, to assess the comparative resistance of different notch detail machining for a 50-year exposure to wind of an intensity that would cause the load in the detail to become close to its loadbearing capacity.

Monotonic testing was used to assess the breaking load of the element, and then this load was used as a basis for constructing a time history representative of 50-year wind exposure with the equivalent effect on the structural integrity of the element as on the breaking load. The chosen load history used in testing was based on the proposal by BRE in 1984, as described by N.J. Cook [8] (Appendix K, Table 1). This load history was appropriate for a 50-year design life in the UK. An alternative load history by Gerhard and Kramer [13], used by UEAtc and ETAG documents, was also considered. Both load histories are similar [14], Cook's load history was chosen as being representative since specimen profiles are used in the UK market.

It should be noted that, due to the mass of a curtain wall and to the stiffness of the frame, the dynamic excitement of wind gusts is irrelevant and may be neglected [15] (6.2.f); therefore, the load history was adequately expressed as a series of monotonic loads. The sequence of steps 1–6 was repeated five times, followed by step 7 (100% of the design load F) (Table 3). A total of 6401 (1280 × 5 + 1) cycles were performed. To represent wind gust, the duration of one cycle was chosen to be 3 s.

Design load F was determined based on the minimal failure load F_{max} of sharp notched specimens from monotonic testing (Table 2). The maximal force for specimen M_N1_1 was equal to 6.78 kN.

The hypothesis was that the aluminium profile would not fail due to fatigue, so a failure load for the profile, F_{max}, corrected for the appropriate partial factor, was chosen for design load F for the load history. According to Eurocode 0 [16], the value of the partial factor for wind action, γ_f, is 1.5. The design force for cyclic testing is then $F = F_{max}/\gamma_f = 6.78/1.5 = 4.50$ kN. The load history for the cyclic testing is provided in Table 4.

Table 4. Load history for cyclic testing.

Loading Step	Number of Cycles	Percentage of the Design Load F	Nominal Load F_i for Step i [kN]
1	1	90%	4.05
2	960	40%	1.80
3	60	60%	2.70
4	240	50%	2.25
5	5	80%	3.60
6	14	70%	3.15
7	1	100%	4.50

2.4.2. Cyclic Test Specimens

Profile specimens were tested [17] using the same apparatus as for monotonic testing, by applying a cycling horizontal point load acting at 15 mm from the top end of the profile. The load history in Table 3 was programmed as a series of sinusoidal load pulses. The series of steps 1–6 was repeated five times, and at the end, step 7 was applied. In total, 7 specimens were tested (see Table 1).

The measured data was collected using a datalogging device that recorded all measurements at 0.01 s intervals. The duration of the cyclic testing for one specimen was approximately 9 h.

Figure 11 shows the diagram of the maximal opening of the notch, expressed as the difference between deflections δ_1 and δ_2 (readings of LVDT_1 and LVDT_2, respectively) for each set of cycles (single Fi) in each series for the specimen with the sharp notch (C_N1_1). It can be noted that there was a slight increase in the opening of the notch ($\delta1$-$\delta2$) after the first series for Fi = 90% F and Fi = 40% F load cycles. This could be caused by the onset of the crack in the root of the notch, but this pattern was not observed on other specimens and there is no definite proof of that hypothesis. For subsequent series of cycle steps, it can be observed that a stable value of measured deflections and slight fluctuations were attributed to the tolerance of the applied force due to the precision limits of the hydraulic press.
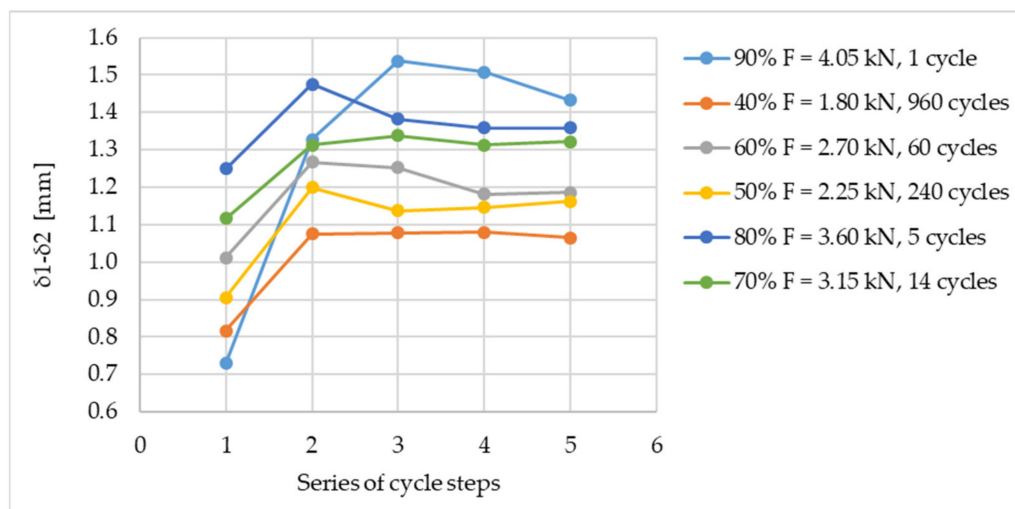

Figure 11. Opening of the notch, sharp notch specimen C_N1_1.

In all 3 specimens with the sharp root notch (C_N1_1, C_N1_2 and C_N1_3), a crack developed at the root of the notch (Figure 12). The stress concentration during the cyclic loading caused the crack propagating 1–2 mm in the direction bisecting the internal corner of the notch, which was in the range of 35° to 55°. The length of the fracture was measured using a microscope Elcometer 900 graduated ×50. It was not possible to identify the cycle at which the crack appeared nor its propagation rate. The apparent slight differences in the colour of surfaces in Figure 12, enlarged details, are due to the light conditions and to residues from the red liquid penetrant used to emphasise surface irregularities; in fact, all samples had the same surface finish.

Cracking of the specimens with the rounded (Figure 13a) and semi-circular roots (Figure 13b), did not occur. In the zone approximately 20 mm around the crack, a net of microcracks radiating from the internal corner of the notch was visible. It is important to note that all specimen surfaces were anodized with aluminium trioxide, which has a higher modulus of elasticity and higher hardness than the parent material below. For high strains, the anodized surface will crack before the alloy material below. It is not uncommon for anodized surfaces with a thickness of around 30 μm or more to experience microcracking caused by the temperature expansion of the parent material. Such a surface becomes "crazed" with crisscrossing lines. This also happened in this test, but due to the high strain. Microcracks are present only in the surface finish (anodization), while the material below was not cracked, apart from a main crack that grew through the full thickness of the aluminium wall and was observable from both sides of the aluminium wall.
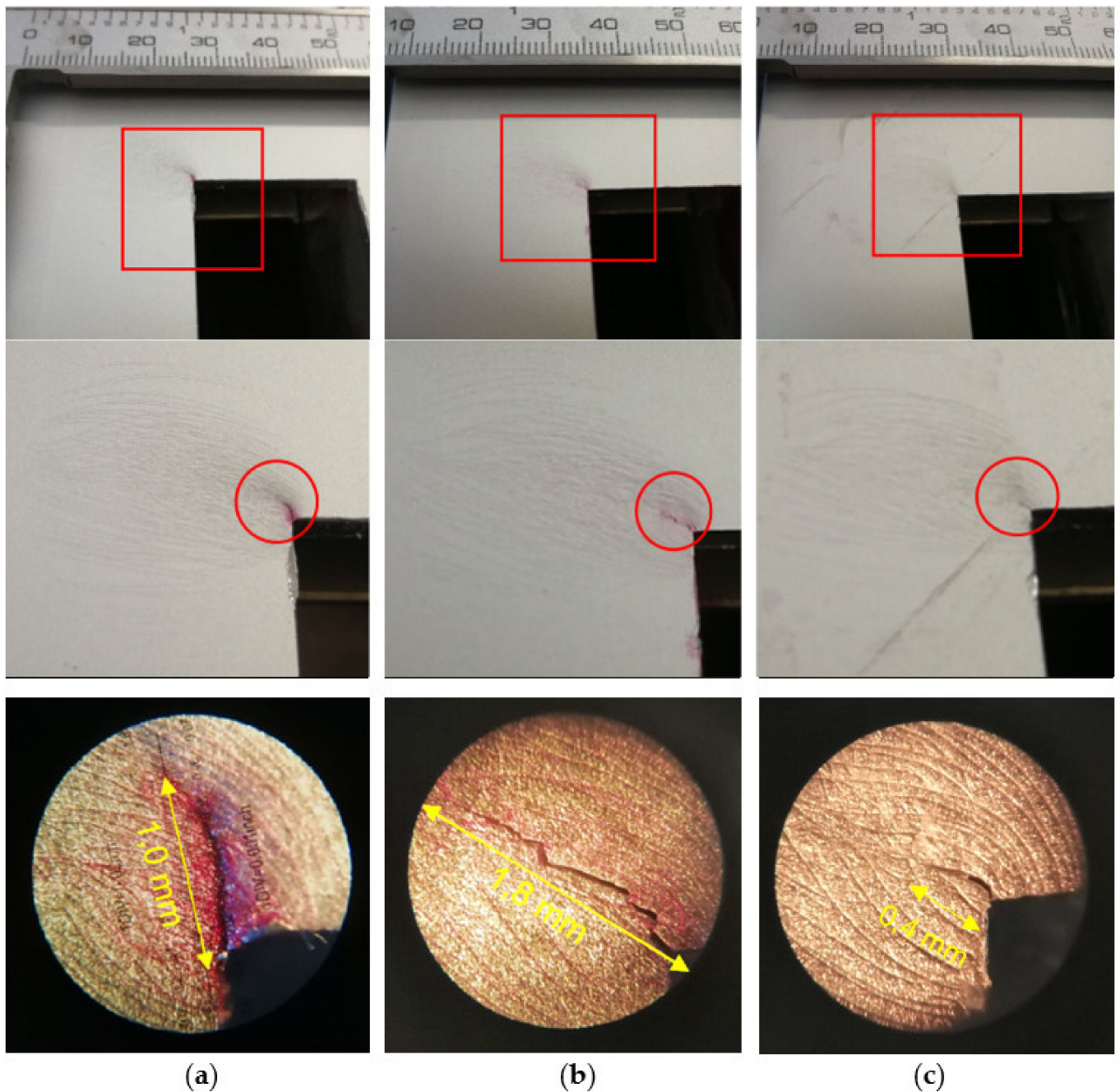
Figure 12. Cracks in specimens with the sharp root: (**a**) C_N1_1, (**b**) C_N1_2, (**c**) C_N1_3.

This microcracking of the surface finish was also visible on specimens with rounded roots and with semi-circular roots. However, on these specimens, no cracks in the aluminium alloy wall occurred. The aluminium material around the root of the notch did under-go a yield, observable from the residual deformation, which is approximately 1 mm at the opening of the notch, but without initiating cracks (Figure 13a,b).
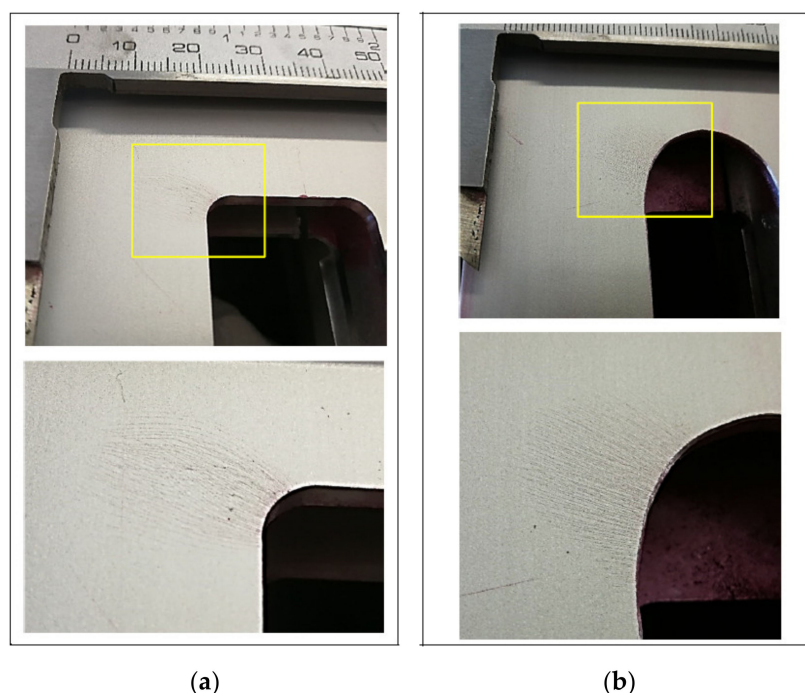
(a)   (b)

Figure 13. Microcracking of the surface of specimens with the rounded and semi-circular root: (a) C_N2_1; (b) C_N3_1.

3. Numerical Analysis

A numerical analysis of the test assembly for all notch geometries was conducted in order to assess the strain and stress distributions in the vicinity of the notch. The depth of the plastic zone around the root of the notch is important for the containment of a crack and the prevention of its further growth. The results of the simulation were compared to measured values for verification purposes so that the modelling can be applied in future analysis of similar details.

The true stress–strain relations, σ_t–ε_t, for the material used (aluminium alloy EN AW 6063 T6 (extrusion)) were calculated from engineering values measured on dog-bone coupons (Table 5), where L_0 is the gauge length, L is the elongated length, A_0 is original cross-section area of the specimen, and A is true cross-section area of the specimen at strain ε:

$$\varepsilon_t = \ln\left(\frac{L}{L_0}\right) = \ln(1 + \varepsilon) \tag{1}$$

$$\sigma_t = \frac{F}{A} = \frac{F}{A_0}\frac{A_0}{A} = \frac{F}{A_0}\frac{L}{L_0} = \sigma(1 + \varepsilon) \tag{2}$$

Table 5. Engineering vs. true stress at the tensile strength.

Coupon	Engineering Stress R_m (MPa)	Corresponding True Stress σ_t (MPa)
Al1	229.8	243.9
Al2	233.7	245.9
Al3	241.9	258.0

Engineering and true stress–strain curves for the dog-bone coupon Al1 are shown on Figure 14. The standardised stress–strain curve for alloy EN AW 6063 T6, defined by [18] (E.2.2.2), is included.

The analysis was performed using material nonlinearity. Two strain–stress curves were used, one true, calculated from tested dog-bone coupon Al1 (chosen, conservatively, for having the lowest strength of all 3 coupons), as per Figure 14, and the other as provided by [18] (E.2.2.2).
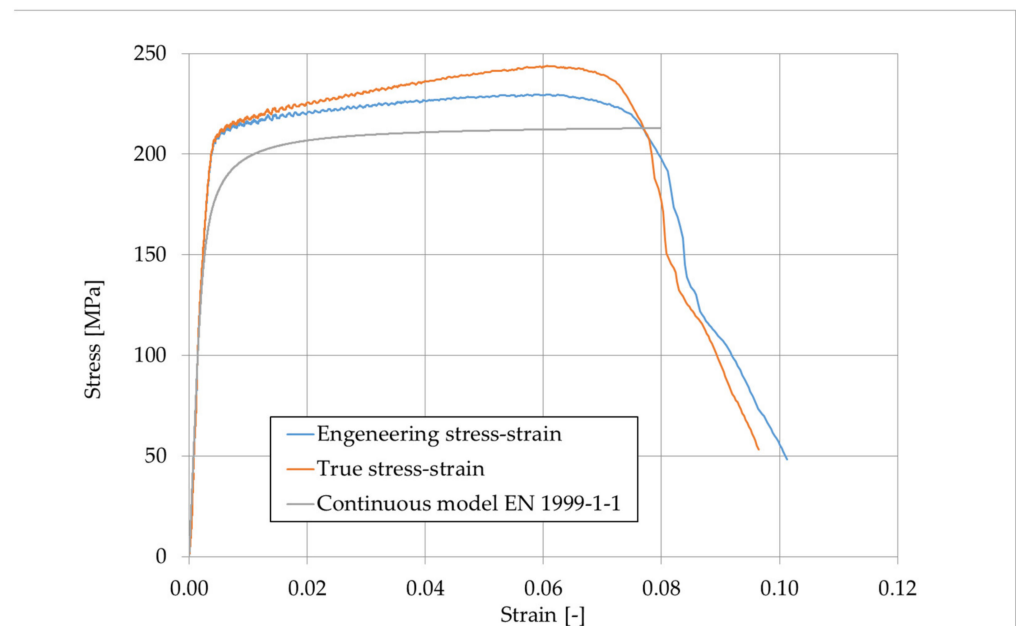
Figure 14. Engineering, true and standardised stress–strain curves for Al1.

Models were loaded by a concentrated horizontal force at the contact point of the actuator. The load was increased in steps of 0.5 kN until the nonconvergence of the solution was reached.

Specimens with all 3 notch geometries were numerically modelled by FEM software Straus7 R2.4.6–Strand7 [19] using solid, 8-node brick elements. The size of elements was 2.5–5 mm, with one element through the thickness of the profile wall (Figure 15a), maintaining the aspect ratio of elements in the zone around the root of the notch higher than 0.4 [20]. In the zone around the notch, the density of the mesh was increased to 2 elements in the thickness of the aluminium wall and the size of the elements was reduced to 0.5–2.5 mm (Figure 15b).
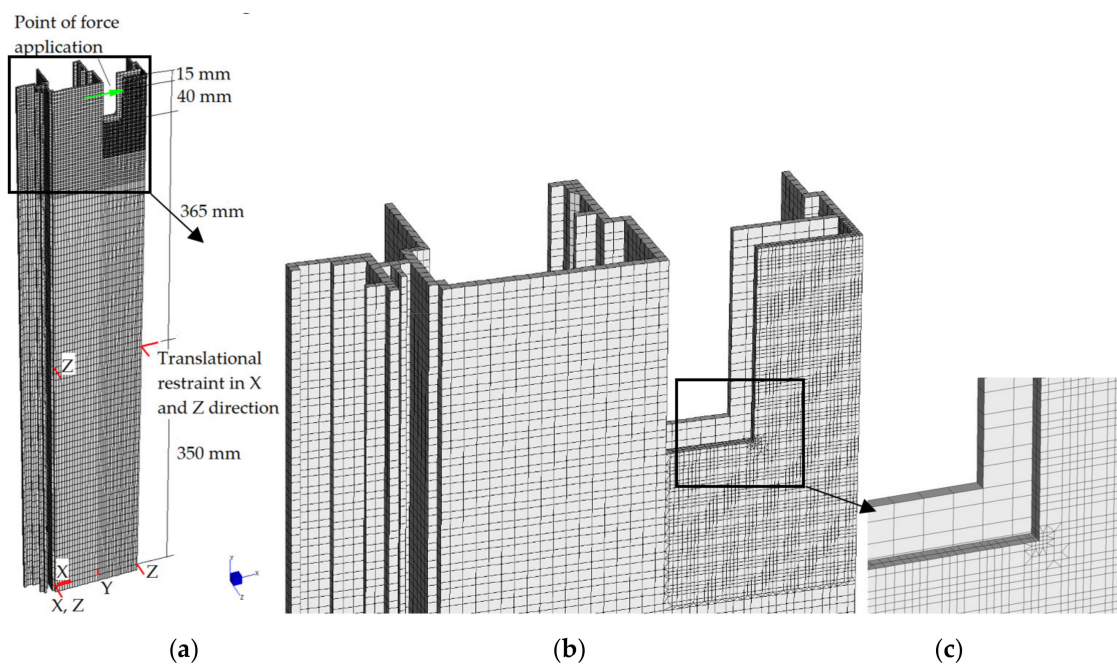

Figure 15. Element mesh: (**a**) entire model, (**b**) upper part, and (**c**) mesh around the root of the notch.

The deformed shape obtained by numerical simulation is shown on Figure 16a, and the deformation of the profile obtained by testing is shown in Figure 16b.
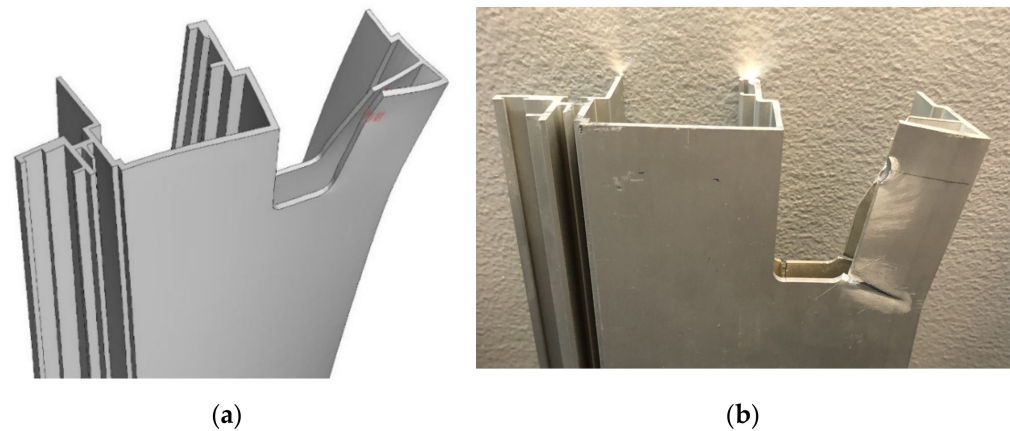

(a)   (b)

Figure 16. Deformed shape of the specimen N1: (**a**) numerically and (**b**) experimentally obtained.

The highest achieved force for models using the true stress–strain curve was 5.5 kN, and the highest achieved force for models using the standardised stress–strain curve (alloy EN AW 6063 T6) was 5.0 kN. Models of the semi-circular notch at 67.5 mm achieved 0.5 kN less force: 5.0 kN and 4.5 kN. The distribution of the strain for all models is shown in Figures 17–20. The wide area of the yielding can be seen (magenta) around the root of the notch.
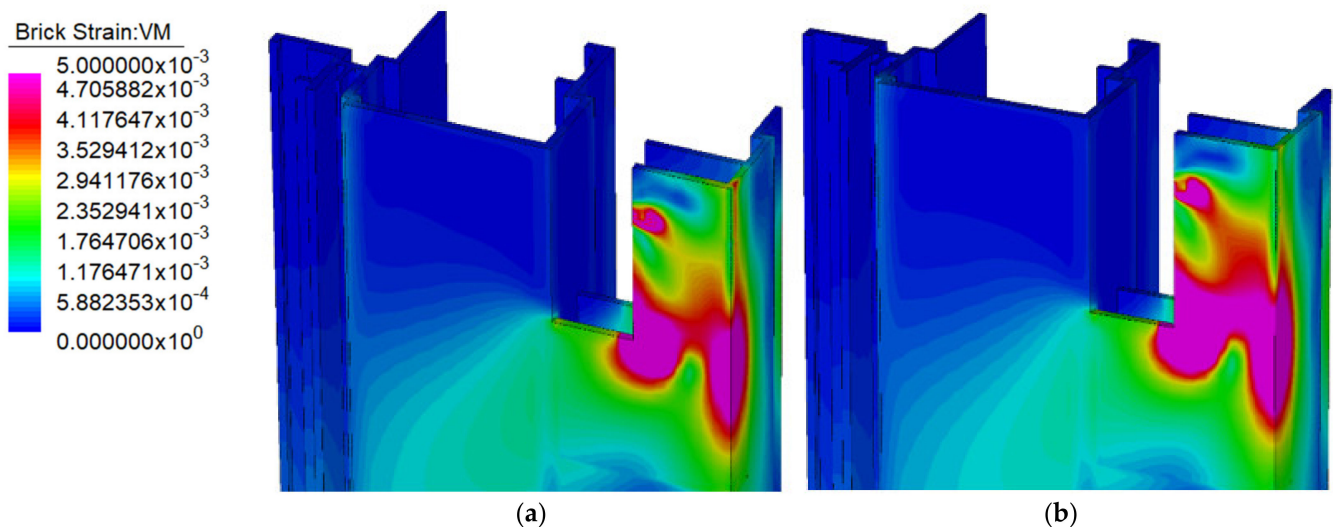

(a)   (b)

Figure 17. Strain in the model of the sharp notch: (**a**) True stress–strain curve (coupon Al1), load 5.5 kN; (**b**) standardised stress–strain curve (alloy EN AW 6063 T6), load 5.0 kN.

For the semi-circular notch, two different geometries were modelled, Figures 19 and 20. The difference between them was the total depth of the notch. Tested specimens had an initial depth of 55 mm, to which a semi-circular machining with a radius of 12.5 mm was performed, resulting in a total depth of 67.5 mm. In order to match the total depth of the other two geometries, an additional model with a semi-circular root was created, which had a total depth of 55 mm, including the semi-circular part, equal to the sharp and rounded notches. Hence, a 67.5 mm notch was representative of tested specimens, whereas a 55 mm notch had the same notch depth as other tested geometries.
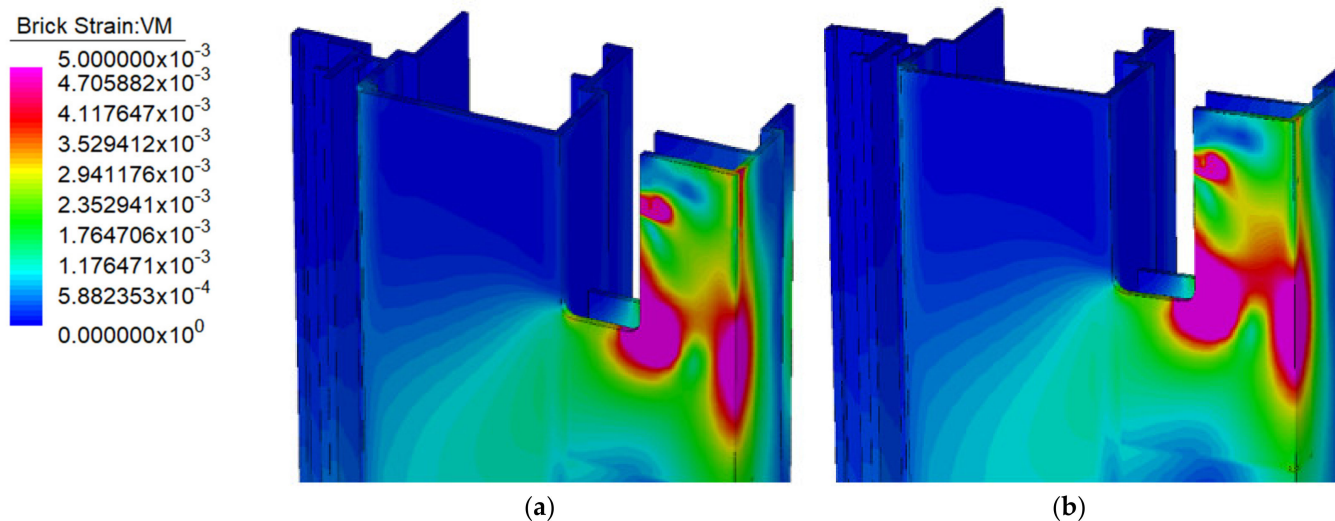
Figure 18. Strain in the model of the rounded notch: (**a**) True stress–strain curve (coupon Al1), load 5.5 kN; (**b**) nominal stress–strain curve (alloy EN AW 6063 T6), load 5.0 kN.
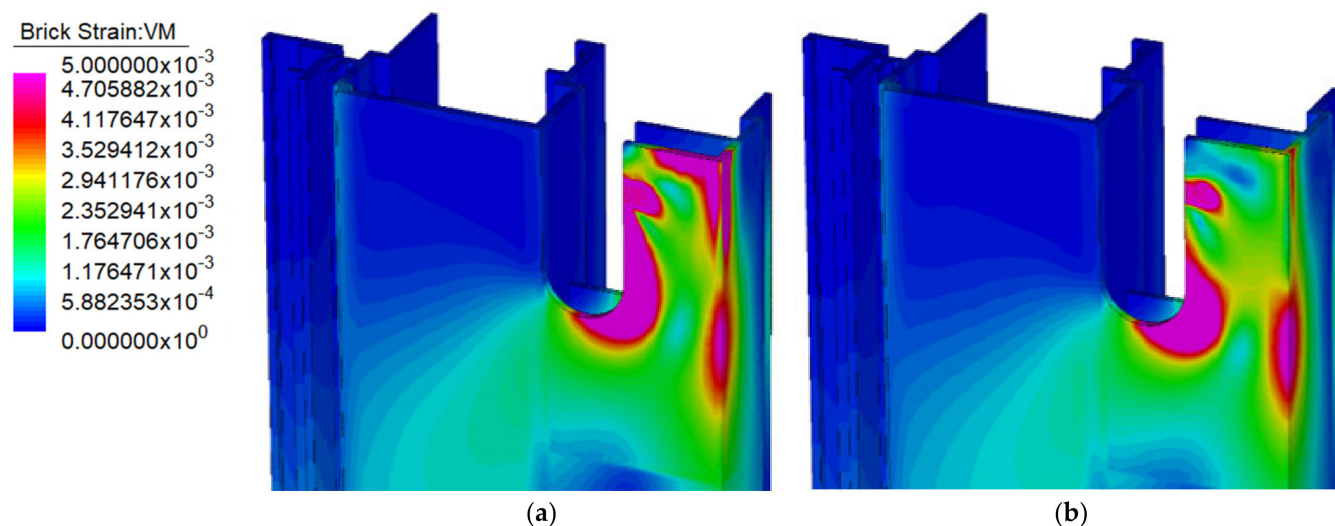

Figure 19. Strain in the model of the semi-circular notch 55 mm: (**a**) True stress–strain curve (coupon Al1), load 5.5 kN; (**b**) nominal stress–strain curve (alloy EN AW 6063 T6), load 5.0 kN.

In general, nonconvergence of numerical models occurred significantly below the measured breaking load, approximately at 80% for the model with the sharp notch, 70% for the rounded notch, and 50% for the semi-circular notch. This can be attributed to the numerical instability at high strain rates. It can be observed that the zone of high strain increased with an increase in the radius at the notch root, which also increased the numerical instability.

Numerical models with the same notch geometry, but with different stress–strain curves, show a similar deflection at the low strain and a small difference at the high strain (Figures 21–23):

- Higher stress for the Al1 true curve, which had higher stress in the plastic zone.
- Higher strains for the standardised curve, which had lower proof stress, thus yielding earlier.

Figure 21 shows that, when a standardised stress–strain curve was used, the highest maximal strains occurred at the sharp notch and the lowest maximal strains occurred at the semi-circular notch.
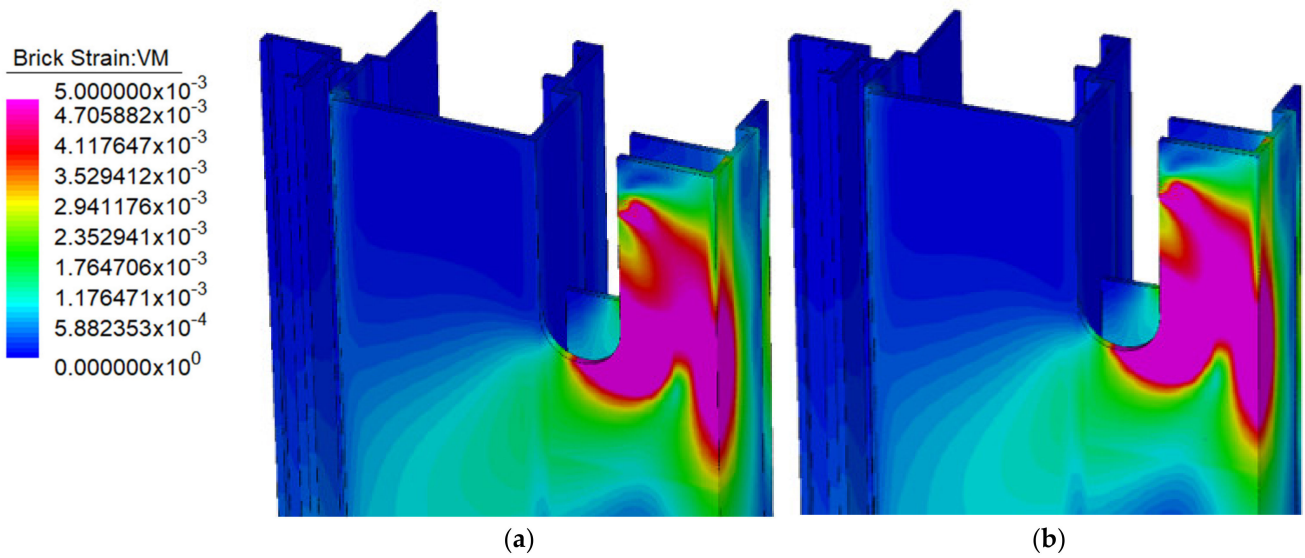
Figure 20. Strain in the model of the semi-circular notch 67.5 mm: (**a**) True stress–strain curve (coupon Al1), load 5.0 kN; (**b**) nominal stress–strain curve (alloy EN AW 6063 T6), load 4.5 kN.

The advantage of a rounded corner on the notch can be seen from the tabulated strain at 5.0 kN load (Table 6). The greater the radius, the less the strain and, as a result, the more resistant the detail.
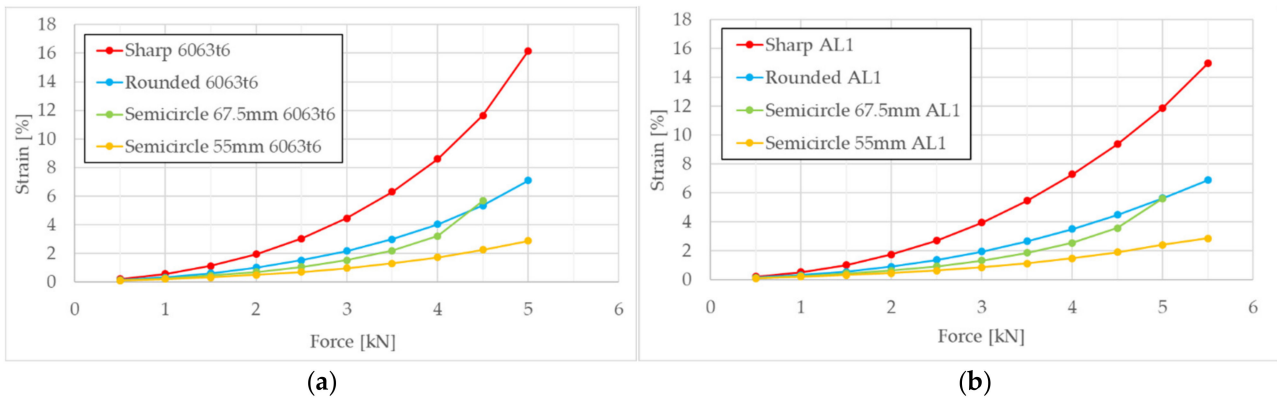

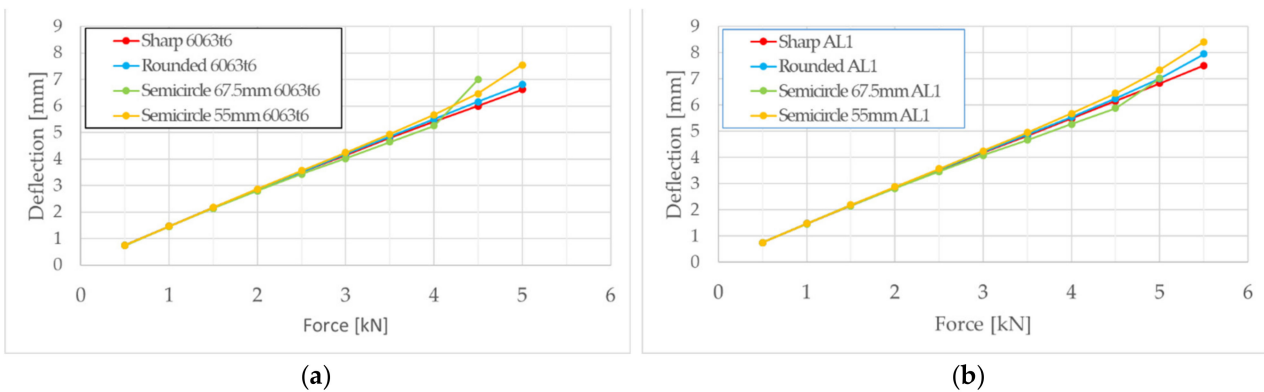**Figure 21.** Strain-force curves for the (**a**) nominal and (**b**) true stress–strain curve.

Figure 22. Deflection-force curves for the (**a**) nominal and (**b**) true stress–strain curves.
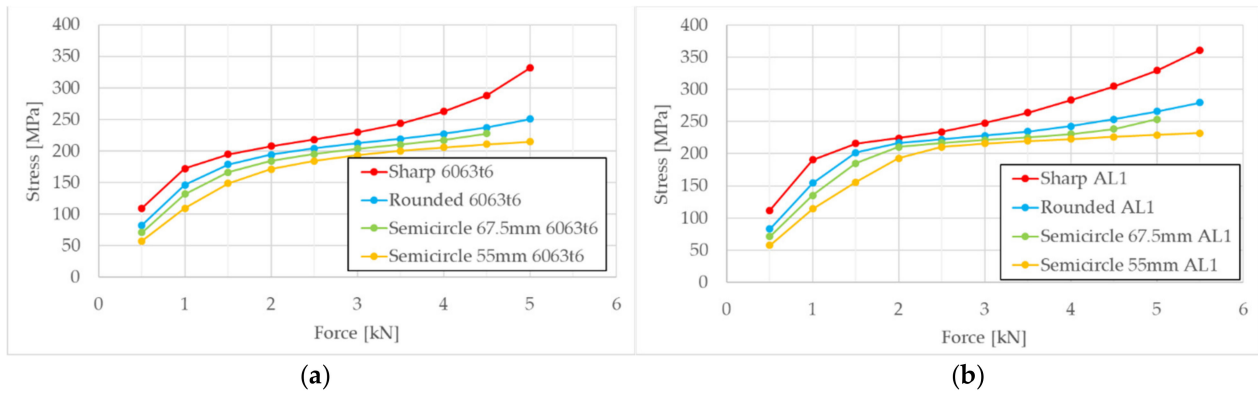
Figure 23. Von Mises stress–strain curves for the (**a**) nominal and (**b**) true stress–strain curves.

Table 6. Numerical modelling—strain at 5.0 kN.

Notch Shape	Strain [%]	
	Nominal Stress–Strain Curve	True Stress–Strain Curve (Al1)
Sharp	16.17	11.88
Rounded	7.10	5.64
Semi-circular (depth 55 mm)	2.88	2.42
Semi-circular (depth 67.5 mm)	5.69 *	5.62

(*) at 4.5 kN (no convergence for 5.0 kN).

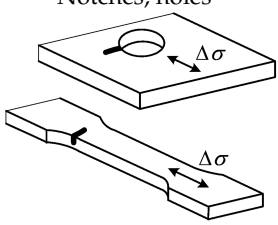## 4. Fatigue Resistance According to Eurocode 9

The fatigue resistance of the element was assessed according to EN 1999-1-3 [21]. The scope of this assessment was only to compare different notch geometries using cumulative linear damage model. According to Annex J [21], the selected detail category is 1.6 with the following parameters (Table 7):

$$\Delta\sigma = 100 \text{ MPa—nominal stress range}$$

$$m_1 = 7\text{—inverse slope constant of } \log\Delta\sigma\text{-}\log N \text{ fatigue strength curve for}$$

$$N \leq 5 \times 10^6 \text{ cycles}$$

Table 7. Detail type 1.6, as per EN 1999-1-3, Table J.1.

Detail Type	Detail Category $\Delta\sigma$-m_1	Product Forms Constructional Detail Initiation Site	Stress Orientation	Stress Analysis	Execution Requirements	
1.6	100-7	Notches, holes / Surface irregularity	Parallel or normal to rolling or extrusion direction.	Account for stress concentration.	Surface free of sharp corners unless parallel to stress direction; edges free of stress raisers	No score marks transverse to stress orientation visual inspection

In tested specimens, the high stress range was applied less than 10^5 times, so the endurance, N_i, could calculated as per [21], according to Annex F for low cycle fatigue range:

$$N_i = \left(\frac{\Delta\sigma_C}{\Delta\sigma_i} \frac{1}{\gamma_{Ff}\gamma_{Mf}} \right)^{m_0} \cdot 20^{\frac{m_0}{m_1}} \cdot 10^5 \tag{3}$$

$\Delta\sigma_c$ = 100 MPa—reference value of fatigue strength at 2×10^6 cycles

R = 0—stress ratio for the cycle range between σ_{min} = 0 and $\sigma_{max} > 0$

For the stress ratio R < +0.5, the enhanced reference fatigue strength $\Delta\sigma_{c(R)}$ is used:

$$\Delta\sigma_{c(R)} = f(R) \, \Delta\sigma_c \tag{4}$$

For R = 0 and for initiation sites away from connections, the enhancement factor f(R) is:

$$f(R = 0) = 1.2 - 0.4 \, R = 1.2 \tag{5}$$

$$\Delta\sigma_{c(R)} = 120 \text{ MPa} \tag{6}$$

$\Delta\sigma_i$—stress range for the principal stresses at the detail, max hotspot stress range at the root of the notch in numerical models, [21]

γ_{Ff} = 1.0—partial factor for fatigue loads, [21]

γ_{Mf} = 1.0—partial factor for materials, [21]

$m_0 = m_1 = 7$—inverse slope of log$\Delta\sigma$-logN curve at $10^3 \leq N \leq 10^5$ cycles

Formula (3) becomes

$$N_i = \left(\frac{120}{\Delta\sigma_i}\right)^7 \cdot 2 \times 10^6 \tag{7}$$

Since the stress history had cycles of various amplitude, the Palmgren–Miner rule was applied in order to assess the total damage D_L:

$$D_L = \sum \frac{n_i}{N_i} \tag{8}$$

where:

n_i—number of cycles of stress range $\Delta\sigma_i$

N_i—endurance under stress range $\Delta\sigma_i$

Number of cycles is defined in Table 4, and the total number of cycles, after the sequence was repeated 5 times, as defined in Table 3, is shown below in Table 8.

Table 8. Total number of cycles.

Cycles	Total of Cycles n_i	Force (kN)
1	5	4.05
960	4800	1.80
60	300	2.70
240	1200	2.25
5	25	3.60
14	70	3.15
1	1	4.50
	6401	

Numerical simulations were performed for the load in steps of 0.5 kN, which did not necessarily match the values of the load used for the cyclic testing (Table 3). In order to assess the hotspot stress range ($\Delta\sigma_i$) for each cycle, the resulting von Mises stresses from the numerical model were used to generate stress–strain curves through the polynomial regression of each notch type. Figure 24 shows the regression curve for the sharp notch. Hotspot stress ranges ($\Delta\sigma_i$) for each cycle were assessed from the obtained curves. Models with the true stress–strain curve for dog-bone coupon Al1 were used.
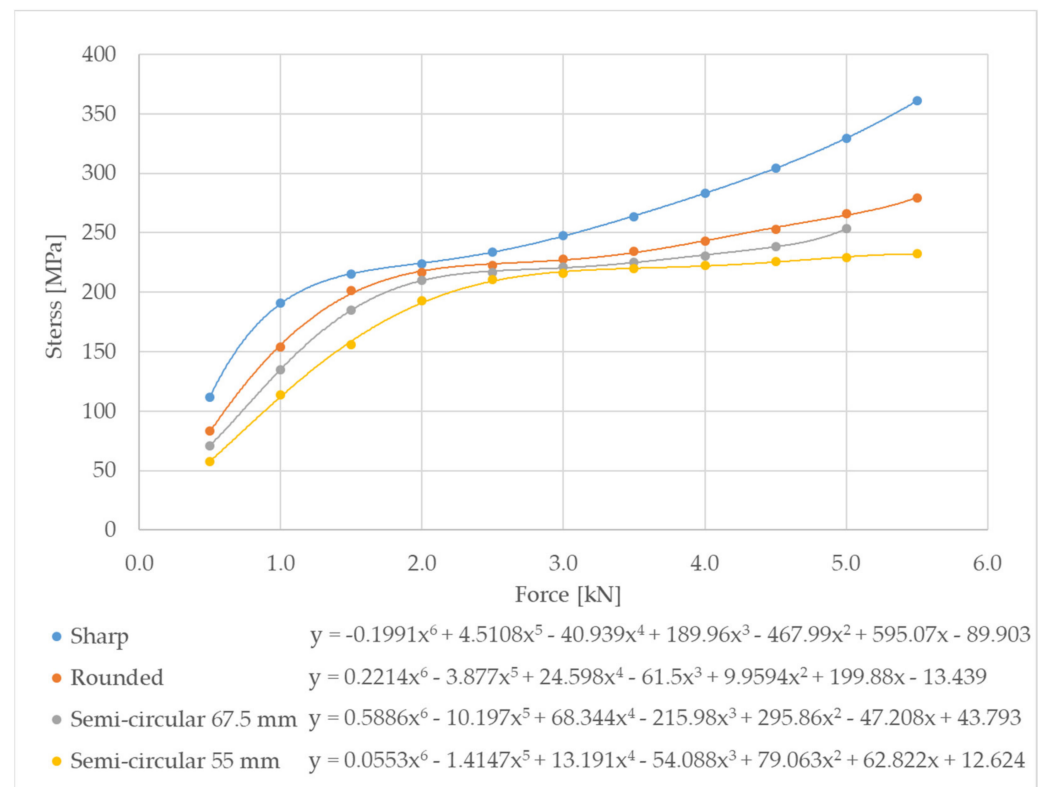
Figure 24. Von Mises stress–strain regression curves for $\Delta\sigma_i$.

For each geometry of the notch, the hotspot stress ($\Delta\sigma_i$) for each cycle was assessed from the respective regression curve. The endurance (N_i) for each cycle was calculated using Formula (7), and the total damage for each cycle was calculated using Formula (8). The results of this procedure for the sharp notch are shown in Table 9.

Table 9. Total damage for the sharp notch.

Cycles n_i	Force [kN]	Stress [MPa]	Endurance N_i	Damage D
5	4.05	285.1	4679	0.00107
4800	1.80	221.5	27,410	0.17512
300	2.70	238.6	16,292	0.01841
1200	2.25	228.6	21,947	0.05468
25	3.60	267.9	7235	0.00346
70	3.15	252.1	11,083	0.00632
1	4.50	304.1	2981	0.00034
6401				0.25939

The total damage, D_L, was 0.259, which is lower than 1.0; therefore, the safe life design was achieved, and it can be assumed that the element was not likely to fail due to fatigue during its design life (T_L) of 50 years. The expected safe life (T_S) is:

$$T_S = T_L / D_L = 193 \text{ years} \tag{9}$$

By applying Formulas (7) and (8), the total damage was assessed for each notch type. The results of the analyses for all notch types are shown in Table 10.

Table 10. Total damage and expected safe life.

Notch Type	Total Damage D_L	Expected Safe Life T_s [Years]
Sharp	0.259	193
Rounded	0.192	260
Semi-circular 55 mm	0.076	660
Semi-circular 67.5 mm	0.144	348

For each calculated geometry of the notch, the number of cycles was too low to cause fatigue failure, even though the stress concentration in the hotspot was higher than the yield limit (0.2% proof strength) for most of the loads. It is expected that the eventual failure will be caused by material failure at the root of the notch, as described by fracture mechanics.

5. Discussion

It was observed that specimens with a rounded or semi-circular notch did not exhibit cracking, although the material at the notch underwent plastic deformation. Specimens with the sharp notch developed a crack early in the cyclic testing, but the crack did not grow further, and the specimen remained stable to the end of the test.

The cause of the cracking was stress concentration. The notch is a geometric stress raiser that causes a localised increase of the stress. Many factors influence the stress concentration, among which, the most important are: geometry of the member, notch radius, basic material characteristics, material homogeneity on the microscopic scale, local plastic deformation, residual stress, and the load type (monotonic, cyclic, impact) [22]. In this paper, only the influence of the notch radius is considered.

It is known that notch sensitivity is small for smaller elements and small radii of the notch, so extremely high theoretical concentration factors for very sharp notches were not actually realised [6]. Furthermore, ductile materials have a low notch sensitivity index due to the local plastic deformation at the notch root. The theoretical peak stress is lowered by plastic action, which redistributes the stress and decreases the effective stress concentration factor [7].

In tested specimens with a sharp notch, this behaviour was observed. The nucleation of the crack happened early during the test, but throughout the entire cycling, it remained stable. It is assumed that the crack remained within the plastic zone (Figure 3), and did not grow out of it. This was confirmed by numerical modelling, which showed that the plastic zone was much deeper (20–40 mm) than the length of the cracks, which were experimentally determined in the range of 1–2 mm; see Figure 12.

6. Conclusions

Three configurations of a detail of an extruded aluminium alloy EN AW 6063 T6 profile were tested to verify the 50-year design service life of a building [23] using a sharp, rounded, and semi-circular notch:

- Specimens were first tested in the monotonic regime until failure in order to assess their maximal load capacity. As expected, specimens with a sharp root had a substantially lower failure load, roughly 20% lower than that of the other specimens.
- Specimens were then tested in the cyclic regime in order to assess their fatigue resistance. The applied variable load history is typical for a 50-year exposure to wind in the UK, which was the actual in-use condition of the original profiles. The selected magnitude of the load history was derived from the lowest monotonic failure load of the specimen with the sharp root, reduced by the partial factor for the wind load.

It was observed that all specimens exhibited microcracks in the surface finish. This has no structural implications and is not deemed to be a failure, but rather, an acceptable working condition. Such microcracks cannot cause the onset of corrosion due to the healing properties of the aluminium and due to its favourable exposure being internal to the air barrier. Specimens with the rounded and semi-circular notches did not exhibit any

cracks throughout the test, so they fulfilled requirements for a safe life according to [21] throughout their design life.

All specimens with the sharp root notch exhibited full-penetration cracks propagating at 45° for a length of 1–2 mm. The crack geometry was consistent in shape for all 3 specimens. It should be noted that the propagation of cracks was very limited to the vicinity of the sharp internal corner and the length of cracks was lower than the thickness of the aluminium wall (2.5 mm). This indicates that such a situation should remain stable for the duration of the building's design service life and that repeated loading would not result in progressive collapse of such a detail. Thus, specimens with a sharp notch fulfil the requirements for the damage-tolerant design according to [21]. Buildings with such a notch design can be deemed safe for use. This reasoning does not take into account other non-structural performance requirements, such as possible breach of the air barrier, possible water penetration, or aesthetical issues related to such a crack.

This conclusion cannot be extended to other designs, since they may differ in choice of alloy, cross-sectional geometry of the profile, notch geometry and its position within the profile, or load history, and, hence, exhibit different behaviour during their design life. For other designs, it is recommended not to use sharp notch geometry without conducting laboratory testing of the notch's sensitivity to fatigue. Sharp internal corners of notches should be avoided in general. However, the gain in the machining costs may justify the effort of testing and the subsequent use of sharp rooted notches in practice.

References

1. Georgantzia, E.; Gkantou, M.; Kamaris, G.S. Aluminium alloys as structural material: A review of research. *Eng. Struct.* **2021**, *227*, 111372. [CrossRef]
2. Lotsberg, I. *Fatigue Design of Marine Structures*; Cambridge University Press: New York, NY, USA, 2016.
3. Gurney, T.R. *Fatigue of Welded Structures*, 2nd ed.; Cambridge University Press: Cambridge, UK, 1979.
4. Forrest, P.G. *Fatigue of Metals*; Pergamon Press: Oxford, UK, 1962.
5. Maljaars, J.; Lukić, M.; Soetens, F. Comparison between the Eurocode for Fatigue of Steel Structures, EN 1993-1-9, and the Eurocode for Fatigue of Aluminium Structures, EN 1999-1-3. *Procedia Eng.* **2013**, *66*, 34–48. [CrossRef]
6. Pilkey, W.D. *Formulas for Stress, Strain, and Structural Matrices*, 2nd ed.; Wiley & Sons, Inc.: Hoboken, NJ, USA, 2005.
7. Fatemi, A. *Notches and Their Effect*; University of Toledo: Toledo, OH, USA, 2011.
8. Cook, J.N. *The Designer's Guide to Wind Loading Structures*; Part 2: Static Structures; BRE: London, UK, 1990.
9. Krolo, P. *Test Report 004/2020: Aluminium Extruded Profiles-Static Test*; Faculty of Civil Engineering University of Rijeka: Rijeka, Croatia, 2020.
10. *EN 755-2:2016 Aluminium and Aluminium Alloys-Extruded Rod/Bar, Tube, and Profiles—Part 2: Mechanical Properties*; European Committee for Standardization: Brussels, Belgium, 2016.
11. Skejić, D.; Dokšanović, T.; Čudina, I.; Mazzolani, F.M. The Basis for Reliability-Based Mechanical Properties of Structural Aluminium Alloys. *Appl. Sci.* **2021**, *11*, 4485. [CrossRef]

12. *EN ISO 6892-1:2016: Metallic Materials–Tensile Testing—Part 1: Method of Test at Room Temperature*; European Committee for Standardization: Brussels, Belgium, 2016.
13. Gerhardt, H.J.; Kramer, C. Wind induced loading cycle and fatigue testing of light-weight roofing fixation. *J. Wind. Eng. Ind. Aerodyn.* **1986**, *23*, 237–247. [CrossRef]
14. Xu, Y.L. Wind-induced fatigue loading on roof cladding of low-rise buildings. In *Cyclone Structural Testing Station: Technical Report No 41*; James Cook University of North Queensland: Townsville, Australia, 1993.
15. *EN 1991:2005 Eurocode 1: Actions on Structures—Part 1–4: General Actions—Wind Actions*; European Committee for Standardization: Brussels, Belgium, 2005.
16. *EN 1990:2002+A1:2005+A1:2005/AC:2010 Eurocode 0: Basis of Structural Design*; European Committee for Standardization: Brussels, Belgium, 2002.
17. Krolo, P. *Test Report 005/2020: Aluminium Extruded Profiles-Fatigue Test*; Faculty of Civil Engineering University of Rijeka: Rijeka, Croatia, 2020.
18. *EN 1999-1-1:2007+A1:2009+A2:2013 Eurocode 9: Design of Aluminium Structures—Part 1-1: General Structural Rules*; European Committee for Standardization: Brussels, Belgium, 2007.
19. Strand7. Available online: https://www.strand7.com/html/docu_usingstrand7.htm (accessed on 20 November 2021).
20. Joshi, A. Stress Concentration Factor Converts into Stress Intensity Factor using ANSYS. *IJSER* **2006**, *7*, 1662–1667.
21. *EN 1999-1-3:2007+A1:2011 Eurocode 9: Design of Aluminium Structures-Part 1–3: Structures Susceptible to Fatigue*; European Committee for Standardization: Brussels, Belgium, 2007.
22. Yen, C.S.; Dolan, T.J. *A Critical Review of The Criteria for Notch Sensitivity in Fatigue of Metals*; Bulletin Series No 398; University of Illinois Engineering Experiment Station: Urbana, IL, USA, 1952.
23. Buljan, N. *Fatigue Testing of the Notch in the Aluminium Profile*; Faculty of Civil Engineering University of Rijeka: Rijeka, Croatia; Faculty of Civil Engineering University of Zagreb: Zagreb, Croatia, 2020.